

Structural basis for the role of serine-rich repeat proteins from *Lactobacillus reuteri* in gut microbe–host interactions

Saannya Sequeira^{a,1}, Devon Kavanaugh^{b,1}, Donald A. MacKenzie^{b,1}, Tanja Šuligoj^b, Samuel Walpole^c, Charlotte Leclaire^b, A. Patrick Gunning^b, Dimitrios Latousakis^b, William G. T. Willats^d, Jesus Angulo^c, Changjiang Dong^{a,2}, and Nathalie Juge^{b,2}

^aBioMedical Research Centre, University of East Anglia, NR4 7TJ Norwich, United Kingdom; ^bThe Gut Health and Food Safety Programme, Quadram Bioscience Institute, NR4 7UA Norwich, United Kingdom; ^cSchool of Pharmacy, University of East Anglia, NR4 7TJ Norwich, United Kingdom; and ^dSchool of Natural and Environmental Sciences, Newcastle University, Newcastle upon Tyne NE1 7RU, United Kingdom

Edited by Scott J. Hultgren, Washington University School of Medicine, St. Louis, MO, and approved January 31, 2018 (received for review August 25, 2017)

Lactobacillus reuteri, a Gram-positive bacterial species inhabiting the gastrointestinal tract of vertebrates, displays remarkable host adaptation. Previous mutational analyses of rodent strain *L. reuteri* 100-23C identified a gene encoding a predicted surface-exposed serine-rich repeat protein (SRRP₁₀₀₋₂₃) that was vital for *L. reuteri* biofilm formation in mice. SRRPs have emerged as an important group of surface proteins on many pathogens, but no structural information is available in commensal bacteria. Here we report the 2.00-Å and 1.92-Å crystal structures of the binding regions (BRs) of SRRP₁₀₀₋₂₃ and SRRP₅₃₆₀₈ from *L. reuteri* ATCC 53608, revealing a unique β-solenoid fold in this important adhesin family. SRRP₅₃₆₀₈-BR bound to host epithelial cells and DNA at neutral pH and recognized polygalacturonic acid (PGA), rhamnogalacturonan I, or chondroitin sulfate A at acidic pH. Mutagenesis confirmed the role of the BR putative binding site in the interaction of SRRP₅₃₆₀₈-BR with PGA. Long molecular dynamics simulations showed that SRRP₅₃₆₀₈-BR undergoes a pH-dependent conformational change. Together, these findings provide mechanistic insights into the role of SRRPs in host–microbe interactions and open avenues of research into the use of biofilm-forming probiotics against clinically important pathogens.

SRRP | *Lactobacillus reuteri* | adhesin | biofilm | mucin

The gastrointestinal (GI) tract of vertebrates is colonized by a complex microbial community dominated by bacteria known as the “gut microbiota.” These bacteria, by having a profound influence on vertebrate physiology, metabolism, and immune functions, play an important role in the health of the host (1). Manipulating the microbiota for the benefit of the host requires an understanding of the molecular mechanisms that govern host–microbe interactions.

Lactobacillus reuteri, a Gram-positive bacterial species that colonizes the gut of a range of vertebrate species, has been used as a model to study host adaptation of gut symbionts (2). The ecological strategies of *L. reuteri* are fundamentally different in humans and animals (3). In rodents, pigs, chickens, and horses, lactobacilli form large populations in proximal regions of the GI tract, and they adhere directly to the stratified squamous epithelium present at these sites (3). In contrast, stratified squamous epithelia are absent in the human gut, where the lactobacilli population is less important and is restricted to the mucus layers and intestinal crypts (3). Genome comparisons of *L. reuteri* strains originating from different hosts identified lineage-specific genomic content that reflects the niche differences in the GI tract of vertebrates (4). Experiments in *Lactobacillus*-free mice to measure the ecological fitness of strains originating from different hosts supported host adaptation, as only rodent strains colonized mice efficiently (5). Furthermore the ability of *L. reuteri* to form epithelial biofilms in the forestomach of monoassociated mice was strictly dependent on the

strain’s host origin (6). Recent studies revealed that rodent strains were particularly successful in colonizing mice, confirming previous findings of host adaptation (7).

The ecological significance of a subset of genes from the rodent-specific *L. reuteri* 100-23C strain was demonstrated in the context of the murine gut (6). This mutational analysis revealed that genes encoding proteins involved in epithelial adherence, specialized protein transport, cell aggregation, environmental sensing, and cell lysis contributed to biofilm formation and colonization (6). In particular, the inactivation of a gene encoding a predicted serine-rich repeat protein (Lr_70902; SRRP₁₀₀₋₂₃) surface adhesin completely abrogated colonization of the mouse forestomach (6). SRRP₁₀₀₋₂₃ is the primary cell wall-associated protein of strain 100-23C that is secreted through an accessory SecA2–SecY2 pathway during *in vivo* growth (6). Recent analysis of the completed genome of pig isolate *L. reuteri* ATCC 53608 revealed the presence of an accessory SecA2–SecY2 secretion system with

Significance

Gut bacteria play a key role in health and disease, but the molecular mechanisms underpinning their interaction with the host remain elusive. The serine-rich repeat proteins (SRRPs) are a family of adhesins identified in many Gram-positive pathogenic bacteria. We previously showed that beneficial bacterial species found in the gut also express SRRPs and that SRRP was required for the ability of *Lactobacillus reuteri* strain to colonize mice. Here, our structural and biochemical data reveal that *L. reuteri* SRRP adopts a β-solenoid fold not observed in other structurally characterized SRRPs and functions as an adhesin via a pH-dependent mechanism, providing structural insights into the role of these adhesins in biofilm formation of gut symbionts.

Author contributions: C.D. and N.J. designed research; S.S., D.K., D.A.M., T.Š., S.W., C.L., A.P.G., and D.L. performed research; W.G.T.W. contributed new reagents/analytic tools; S.S., D.K., D.A.M., T.Š., S.W., C.L., A.P.G., D.L., J.A., C.D., and N.J. analyzed data; and S.S., D.K., D.A.M., T.Š., S.W., A.P.G., J.A., C.D., and N.J. wrote the paper.

The authors declare no conflict of interest.

This article is a PNAS Direct Submission.

This open access article is distributed under Creative Commons Attribution-NonCommercial-NoDerivatives License 4.0 (CC BY-NC-ND).

Data deposition: The structure factors and coordinates reported in this work have been deposited in the Protein Data Bank (PDB), www.pdb.org [accession ID codes 5NKK (SRRP₅₃₆₀₈-BR) and 5NY0 (SRRP₁₀₀₋₂₃-BR)].

¹S.S., D.K., and D.A.M. contributed equally to this work.

²To whom correspondence may be addressed. Email: c.dong@uea.ac.uk or nathalie.juge@quadram.ac.uk.

This article contains supporting information online at www.pnas.org/lookup/suppl/doi:10.1073/pnas.1715016115/-DCsupplemental.

an associated SRRP that shared the same domain organization as SRRP₁₀₀₋₂₃ (8).

SRRPs belong to a growing family of adhesins in Gram-positive bacteria that mediate attachment to a variety of host and bacterial surfaces, and many of them are virulence factors that contribute to bacterial pathogenesis and biofilm formation (9). SRRPs are characterized by (i) two heavily glycosylated serine-rich regions (SRRs), (ii) one or two species-unique nonrepeat regions [NR domains, which include the binding region (BR) domain] toward the N terminus that facilitate specific interactions with a diverse array of host receptors and share little sequence homology to each other, and (iii) a C-terminal cell wall anchor domain (9, 10). Export of SRRPs onto the bacterial surface occurs through a dedicated noncanonical Sec translocase, Sec-Y2A2, following recognition of an extended atypical signal sequence peptide of around 90 aa at the N terminus (10, 11). The domain organization of SRRPs is highly conserved in pathogenic streptococci and staphylococci and includes Srr-1 and Srr-2 of *Streptococcus agalactiae*, PsrP of *Streptococcus pneumoniae*, Fap1 of *Streptococcus parasanguinis*, GspB and Hsa of *Streptococcus gordonii*, SraP of *Staphylococcus aureus*, and SrpA homologs from *Streptococcus sanguinis* and *Streptococcus crista-* *tus* (9, 12, 13). However, the structure and function of SRRPs in gut commensal bacteria have not yet been determined. Here we used a number of complementary approaches to provide a structural basis for the role of *L. reuteri* SRRPs (*L*_rSRRPs) in bacterial adaptation to the host. We show that the *L*_rSRRP-BR adopts a right-handed parallel β-helical or “β-solenoid” fold not observed in other structurally characterized SRRPs and functions as an adhesin via a pH-dependent mechanism. These findings provide insights into the role of *L*_rSRRPs in biofilm formation and structural insights into intra- and interspecies adhesins across Gram-positive pathogenic and commensal bacteria.

Results

Bioinformatics Analysis of SRRPs from Lactobacilli. SRRPs and corresponding specialized secretion systems are being defined in a growing number of pathogens, but their occurrence and characterization in commensal bacteria have been reported only infrequently (14, 15). Our bioinformatics analysis of lactobacilli genomes revealed genes encoding fully functional SRRPs and SecA2-SecY2 secretion systems in a number of *Lactobacillus* species, including strains of *L. reuteri*, *Lactobacillus oris*, *Lactobacillus salivarius*, *Lactobacillus johnsonii*, and *Lactobacillus fructivorans*, with none found so far in other major lactobacilli species such as *Lactobacillus plantarum* (*SI Appendix*, Table S1). In other cases, strains possessed what appeared to be only an incomplete SecA2-SecY2 gene cluster, a SRRP that lacked a C-terminal cell wall anchor (possibly the result of a pseudogene capable of exporting a SRRP extracellularly which would not be covalently linked to the cell surface), or an obvious pseudo-SRRP whose domains were encoded by at least two adjacent ORFs. These include strains of *Lactobacillus gasseri*, *Lactobacillus rhamnosus*, *Lactobacillus murinus*, *Lactobacillus nagelii*, and *Lactobacillus mucosae*, a species closely related to *L. reuteri* (*SI Appendix*, Table S1) (16). When some strains of lactobacilli harbor two SRRPs, at least one of them is encoded by pseudogene fragment(s), highlighting their loss of function due to lack of selective pressure.

Analysis of 58 available genome-sequenced *L. reuteri* strains showed that homologs of functional SRRPs (and the corresponding linked SecA2-SecY2 gene cluster) were found exclusively in some rodent and pig isolates with the exception of one chicken strain and one sourdough strain [previously reported to be of intestinal origin with a genome content similar to that of the model rodent isolate 100-23 (17)] (*SI Appendix*, Table S2). The putative *L*_rSRRPs from *L. reuteri* rodent strain 100-23C (SRRP₁₀₀₋₂₃) and pig strain ATCC 53608 (SRRP₅₃₆₀₈) possess a

LPXTG cell wall anchor and display characteristics of a protein secreted through the SecA2-SecY2 system, i.e., the presence of an unusually long N-terminal signal peptide and two extremely serine-rich regions, SRR-1 and SRR-2, the second of which contains many repeat motifs (Fig. 1).

Further comparative sequence analysis of SRRP-BR domains was carried out in a total of 76 lactobacilli SRRPs/pseudo-SRRPs and 18 pathogen/clinical-associated SRRPs to generate a neighbor-joining phylogram (*SI Appendix*, Fig. S1). In the case of most *L. reuteri* strains, SRRP-BRs formed groups relating to the host or source from which the strain was isolated, such as the two main groups of pig-derived SRRP-BRs/pseudo-SRRP-BRs and the one main group of rodent/sourdough-derived BRs. Similar relationships were observed for the BRs from *L. oris*, *L. salivarius*, and the pathogenic streptococcal BRs. There were a few exceptions where SRRP-BRs/pseudo-SRRP-BRs of *L. reuteri* strains crossed this host-specific divide, such as the relatedness of (i) the pseudo-SRRP-BRs from rodent strains lpuph, LR0, and TD1 and a number of pig strain SRRP-BRs; (ii) the SRRP-BR from chicken isolate 1366 and the pseudo-SRRP-BRs from three pig strains KLR2001, KLR3005, and pg-3b; and (iii), most importantly, the BR domain from SRRP₁₀₀₋₂₃ of rodent origin and one group of porcine SRRP-BRs that included SRRP₅₃₆₀₈-BR. The SRRP₅₃₆₀₈-BR and SRRP₁₀₀₋₂₃-BR shared ~49% amino acid identity. This compares with the very low amino acid identity of <15% between SRRP₅₃₆₀₈-BR or SRRP₁₀₀₋₂₃-BR and pathogenic bacterial BRs such as GspB-BR, Fap1-NR α , Hsa-BR, PsrP-BR, Srr-1-BR, and Srr-2-BR. Typically, SRRP-BRs from different *Lactobacillus* spp. showed low homology between each other, but one exception was the pseudo-SRRP-BR from *L. mucosae* pig strain LM1 and the predominantly pseudo-SRRP-BRs from 18 *L. reuteri* pig strains and one *L. reuteri* bovine strain, providing some insight into the evolutionary relationships between these two related species (16, 18). We confirmed the presence of the full-length *srp* gene in five pig strains of *L. reuteri* by PCR and showed that the encoded SRRPs were also secreted extracellularly, as previously shown for SRRP₁₀₀₋₂₃ during growth *in vitro* (*SI Appendix*, Fig. S2) (6).

Crystal Structures of *L. reuteri* SRRP-BR Reveal a Unique Fold Within the SRRP Family. SRRP₅₃₆₀₈-BR and SRRP₁₀₀₋₂₃-BR crystals were obtained via *in situ*-limited proteolysis of the full-length *L*_rSRRP-BR proteins with α-chymotrypsin and thermolysin, respectively. The structure of SRRP₅₃₆₀₈-BR was determined at 1.92-Å resolution between residues 262 and 571, excluding 39 and 97 residues from the N and C termini, respectively (Fig. 2A). The structure of SRRP₁₀₀₋₂₃-BR was determined at a resolution of 2.00 Å. The



Fig. 1. Schematic showing domain organization of precursor SRRPs from *L. reuteri*. The two proteins are drawn to scale. Domains are labeled as follows: A, cell wall anchor including LPXTG motif; N1, nonrepeat region 1; N2 (BR), nonrepeat region 2 (putative binding region); N3, nonrepeat region 3; S, secretion signal sequence; SRR-1, serine-rich region 1; SRR-2, serine-rich region 2. The beginning amino acid position is indicated below each domain. Regions of the BR that were resolved by crystallography are shaded gray and span amino acids 257–623 for SRRP₁₀₀₋₂₃ and amino acids 262–571 for SRRP₅₃₆₀₈.

model contains residues 257–623, excluding 55 and 64 residues from the N and C termini, respectively. There are two gaps in the structure (indicated by black spheres in Fig. 2B) which could not be modeled. The first gap of nine residues is from amino acids 413–421, and the second gap of 16 residues is from amino acids 568–583. The data collection and refinement statistics for SRRP₅₃₆₀₈-BR and SRRP₁₀₀₋₂₃-BR are provided in Table 1.

Overall fold of LrSRRP-BRs. The structures of SRRP₅₃₆₀₈-BR₂₆₂₋₅₇₁ and SRRP₁₀₀₋₂₃-BR₂₅₇₋₆₂₃ share 43% sequence identity with an rmsd of 0.912 over 293 aligned C α atoms. Both structures adopt a solenoid-type fold comprising β -strands coiled in a repetitive pattern to form a right-handed helix with three parallel β -sheets (Fig. 2). A Dali search (19) revealed structural homology of LrSRRP-BRs with proteins predominantly belonging to CATH superfamilies 2.160.20.10 and 2.160.20.20 (20). These include pectate lyase C (PelC)-like proteins with right-handed β -superhelical topology (21, 22) such as PelC from the plant pathogen *Dickeya didantii*, the first parallel β -helix protein to be reported (23). Other examples include pectate lyases from *Bacillus* spp. [BsPel, Pel15, and Bsp165PeLA (24–27)], those from *D. didantii* (previously known as “*Erwinia chrysanthemi*”) (Pel9A and PelI) (28–30) and from *Thermatoga maritima* (TM-Pel) (31); pectin lyases from *Aspergillus niger* (PeLA and PeLB) (32, 33), and a rhamnogalacturonase from *Aspergillus aculeatus* (RGaseA) (34).

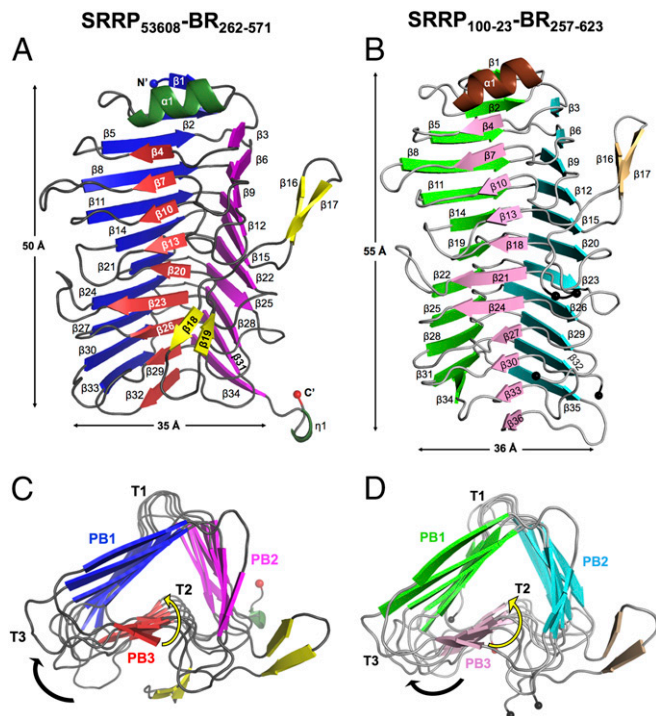


Fig. 2. Crystal structures of SRRP₅₃₆₀₈-BR₂₆₂₋₅₇₁ and SRRP₁₀₀₋₂₃-BR₂₅₇₋₆₂₃. (A) Longitudinal view of SRRP₅₃₆₀₈-BR₂₆₂₋₅₇₁. The β -strands in putative binding regions PB1, PB2, and PB3 are shown in deep blue, magenta, and red, respectively; α -helices are dark green, and β -strands of the loop are yellow. (B) Longitudinal view of SRRP₁₀₀₋₂₃-BR₂₅₇₋₆₂₃. PB1, PB2, and PB3 β -strands are in light green, cyan, and pink, respectively. The α -helix is in brown, and loop β -strands are in beige. The black spheres indicate the gaps in the model between amino acids 413–421 and 568–583. (C) and (D) Cross-sections of SRRP₅₃₆₀₈-BR₂₆₂₋₅₇₁ (C) and SRRP₁₀₀₋₂₃-BR₂₅₇₋₆₂₃ (D) β -solenoid superhelices along the helical axis from the N to the C terminal. In both, β 1 and α 2 are omitted for clarity. The black arrow shows the direction in which the polypeptide chains fold around the helical axis, yielding a right-handed superhelix. The helical twist down each β -sheet is indicated by yellow arrows. Along the helical axis, the β -strands in each parallel β -sheet increasingly twist toward the left with respect to each other.

These enzymes all act on pectin, a structural polysaccharide of plant cell walls (35). The structures of LrSRRP-BRs are strikingly similar to those of PelC-like proteins with rmsds ranging from 2.38 to 3.37 Å over 164–233 aligned C α atoms, despite sharing only 8–23% sequence identity. As shown in Fig. 2 C and D, the parallel β -sheets of LrSRRP-BRs are labeled as “PB1,” “PB2,” and “PB3,” and the disordered turns connecting consecutive β -strands are referred to as “T1,” “T2,” and “T3,” following the convention of Yoder et al. (36). Other shared structural features include (i) amino acid stacks; (ii) an anti-parallel β -sandwich arrangement between PB1 and PB3 to which PB2 is perpendicular; and (iii) the protrusion of flexible domains from the core β -solenoid body, which is often involved in ligand binding. In SRRP₅₃₆₀₈-BR₂₆₂₋₅₇₁ and SRRP₁₀₀₋₂₃-BR₂₅₇₋₆₂₃, this flexible domain takes the form of a two-winged propeller-like loop which originates from β 15 in PB2 (the upper loop) and folds back into β 20 and β 18, respectively, in PB3 (the lower loop).

The Dali search also revealed structural similarity to certain extracellular adhesive proteins with PelC-like folds, such as pertactins and bacteriophage tail-spike proteins (SI Appendix, Table S3). The structure of SRRP₅₃₆₀₈-BR₂₆₂₋₅₇₁ displays an rmsd of 2.81 Å over 220 aligned C α atoms and 3.48 Å over 190 aligned C α atoms to P.69 pertactin and phage P22 TSP, respectively. P.69 pertactin from the pathogen *Bordetella pertussis* facilitates adhesion to mammalian epithelial proteins via a conserved Arg-Gly-Asp motif and two proline-rich regions (37). Phage P22 TSP is an endorhamnosidase acting on the O-antigen of *Salmonella typhimurium*; sugar-binding features observed from the structure of the TSP-O-antigen complex are hydrophobic stacking of aromatic sidechains with sugar pyranose and H-bonds to polar and ionic sidechains (38). Another β -superhelical extracellular adhesive protein is the N-terminal TPS fragment (30 kDa) of a mature filamentous hemagglutinin protein (39) from *Bordetella* spp., which also has an Arg-Gly-Asp motif that recognizes macrophage CR3, a heparin-binding domain, as well as a carbohydrate-recognition domain, for adhesion to lung epithelial cilia (rmsd of 3.18 Å to SRRP₅₃₆₀₈-BR₂₆₂₋₅₇₁ over 197 aligned C α atoms) (40). However, no such Arg-Gly-Asp motif was identified in any of the LrSRRP-BR proteins.

Putative binding sites of LrSRRP-BRs. Superposition of the SRRP₅₃₆₀₈-BR₂₆₂₋₅₇₁ structure with that of pectate lyase TM-Pel in complex with trigalacturonic acid (TGA) (Fig. 3C) revealed a potential binding site in LrSRRP-BRs. In TM-Pel, predominantly basic residues maintain polar contacts and salt bridges with the acidic TGA molecule as shown in Fig. 3B. In SRRP₅₃₆₀₈-BR, the area under the lower loop corresponds to TM-Pel’s binding site and has four basic solvent-exposed residues (K377 on T3 adjacent to β 13 and a triad, K485, R512, and R543, on β 26, β 29, and β 32, respectively), one acidic residue (D487 on β 26), and four solvent-exposed aromatic residues (a triad of W375, Y425, and W450 on β 13, β 20, and β 23, respectively, and Y482 on T2, next to β 26) (Fig. 3D). Given the role of these charged and aromatic residues for sugar binding in PelC-like proteins, the aforementioned surface-exposed residues are postulated to form a putative binding site (PuBS) in SRRP₅₃₆₀₈-BR. The positions of Y482 and R512 in the PuBS are conserved with TM-Pel’s binding site. Superposition of SRRP₁₀₀₋₂₃-BR₂₅₇₋₆₂₃ upon SRRP₅₃₆₀₈-BR₂₆₂₋₅₇₁ revealed a high degree of conservation of amino acid residues between their PuBSs (depicted in Fig. 3E). However, the most notable difference is that the lower loop in SRRP₁₀₀₋₂₃-BR₂₅₇₋₆₂₃ is five amino acids longer and includes two aromatic residues, H414 and Y415, although it could not be modeled in the crystal structure. In addition, solvent-accessible surface electrostatic potential maps of SRRP₅₃₆₀₈-BR₂₆₂₋₅₇₁ and SRRP₁₀₀₋₂₃-BR₂₅₇₋₆₂₃ revealed that, like the TM-Pel binding site, the PuBS in SRRP₅₃₆₀₈-BR₂₆₂₋₅₇₁ is enveloped by positive electrostatic potential (SI Appendix, Fig. S3), whereas the corresponding region in SRRP₁₀₀₋₂₃-BR₂₅₇₋₆₂₃ is acidic, although this may be due to

Table 1. Data collection and refinement statistics for SeMetSRRP₅₃₆₀₈-BR, SRRP₅₃₆₀₈-BR, and SRRP₁₀₀₋₂₃-BR

Protein	SeMetSRRP ₅₃₆₀₈ -BR	SRRP ₅₃₆₀₈ -BR	SRRP ₁₀₀₋₂₃ -BR
Data collection statistics			
Protein Data Bank ID		5NXK	5NY0
Beamline	i04	i03	i04
Wavelength, Å	0.9792	0.9762	0.9002
Space group	P 3 ₂ 2 1	P 3 ₂ 2 1	H 3 2
Cell parameters: a, b, c, Å	148.40, 148.40, 110.73	146.70, 146.70, 110.42	162.36, 162.36, 146.78
α, β, γ, °	90, 90, 120	90, 90, 120	90, 90, 120
Resolution, Å	74.20–2.73 (2.80–2.73)	73.35–1.92 (1.95–1.92)	63.40–2.00 (2.05–2.00)
I/σI	29.7 (6.2)	9.9 (2.2)	16.8 (2.2)
Unique reflections	37,723 (2,781)	104,897 (5,168)	50,080 (3,650)
Completeness, %	99.9 (99.9)	100.0 (99.6)	100.0 (99.9)
Multiplicity	39.0 (40.9)	18.0 (15.5)	9.2 (9.5)
R _{merge}	0.134 (1.134)	0.278 (3.087)	0.061 (0.945)
R _{meas}	0.136 (1.148)	0.286 (3.191)	0.069 (1.060)
R _{pim}	0.022 (0.178)	0.067 (0.797)	0.031 (0.472)
CC _{1/2}	1.000 (0.984)	0.997 (0.668)	0.998 (0.714)
Refinement Statistics			
Molecules per asymmetric unit	3	3	1
Total atoms		7,896	2,786
Water molecules		999	200
R _{factor}		0.1570(0.2458)	0.2241(0.2116)
R _{free}		0.1825(0.2680)	0.2445(0.2517)
Ramachandran analysis			
Most favored		95.90	94.10
Allowed		2.99	4.70
Outliers		0.11	1.20
Rmsd			
Bonds, Å		0.008	0.013
Angles, °		1.240	1.400
Mean atomic B-factor, Å ²		30.60	48.40
Molprobity score	1.36 (98th percentile)	1.60 (94rd percentile)	
Clashscore	2.98 (99th percentile)	3.98 (99th percentile)	

the absence of the (unmodeled) loop in SRRP₁₀₀₋₂₃-BR_{257–623}. Indeed, removing the lower loop in the SRRP₅₃₆₀₈-BR_{262–571} model from F411–T422 led to a reduced positive surface charge around the PuBS (*SI Appendix*, Fig. S3), implying that the residues in this loop may play a role in maintaining the basicity of the PuBS.

Molecular Dynamics Simulations Suggest a pH-Dependent Conformational Change in the L_rSRRP-BR PuBS. Starting from the crystal coordinates of SRRP₅₃₆₀₈-BR_{262–571}, hydrogen atoms were added to the structure according to known protein chemistry (*Methods*). This included prediction of the protonation state of acidic and basic residues at both pH 4.0 and 7.4. The resulting models differed in that 14 acidic residues (E263, E269, D334, E338, E400, E409, E434, D448, E475, E481, D487, E518, E527, and E566) were protonated at the carboxylate sidechain at pH 4.0 (*SI Appendix*, Fig. S4). Furthermore, four histidine residues (H311, H413, H493, and H535) were singly protonated at either the δ- or ε-nitrogen positions at pH 7.4 but were protonated at both positions at pH 4.0. Five of these residues (H413, D448, E481, D487, and E518) are in close proximity to the PuBS. As a result, the PuBS exhibits a more positive surface electrostatic potential at pH 4.0 (Fig. 4 and *SI Appendix*, Fig. S5), which is expected to facilitate binding to anionic polysaccharides at this pH. Furthermore, the majority of differentially protonated residues were found on the surface of SRRP₅₃₆₀₈-BR_{262–571}, which predicts an interruption of key interactions between symmetry-related molecules, potentially explaining why no crystallization could be achieved at pH 4.0 (*SI Appendix*, Fig. S4).

Molecular dynamics (MD) simulations in the microsecond timescale revealed a pH-dependent conformational change in the loop connecting β30 and β31, close to the PuBS, resulting in greater solvent exposure of putative binding residues (Fig. 4). This change is caused by rotation about the Cα-C bond (ψ) of I514 so as to facilitate hydrogen bond formation between the backbone carbonyl of I514 and the hydroxyl of the D487 carboxylic sidechain (*SI Appendix*, Fig. S6). This is possible only at pH 4.0 due to the protonation of the D487 carboxylate group. Furthermore, a resulting reduction in steric interactions between I514 and R512 led to subtle sidechain rearrangements of R512 and Y482 (*SI Appendix*, Fig. S7), which may prearrange these residues for ligand recognition.

SRRP₅₃₆₀₈-BR Displays Specific Binding to Polyanionic Ligands via a Low-pH Mode of Adhesion. Glycan arrays were first used in an attempt to identify the potential ligands of L_rSRRP-BR. Due to the reported binding specificity of several SRRP-BRs from Gram-positive pathogenic bacteria to sialylated structures, we first tested the binding of SRRP₅₃₆₀₈-BR against a sialoglycan microarray presenting over 70 synthetically recreated, naturally occurring oligosaccharide structures with diverse sialic acid forms, glycosidic linkages, and underlying glycans (41, 42) using sodium acetate buffer (pH 4.0) or sodium phosphate buffer (pH 7.4). However, no significant binding was observed under the tested conditions. No significant binding was detected at neutral pH using version 5.1 mammalian glycan arrays from the Consortium for Functional Glycomics (CFG) that contain 610 distinct potential glycan receptors.

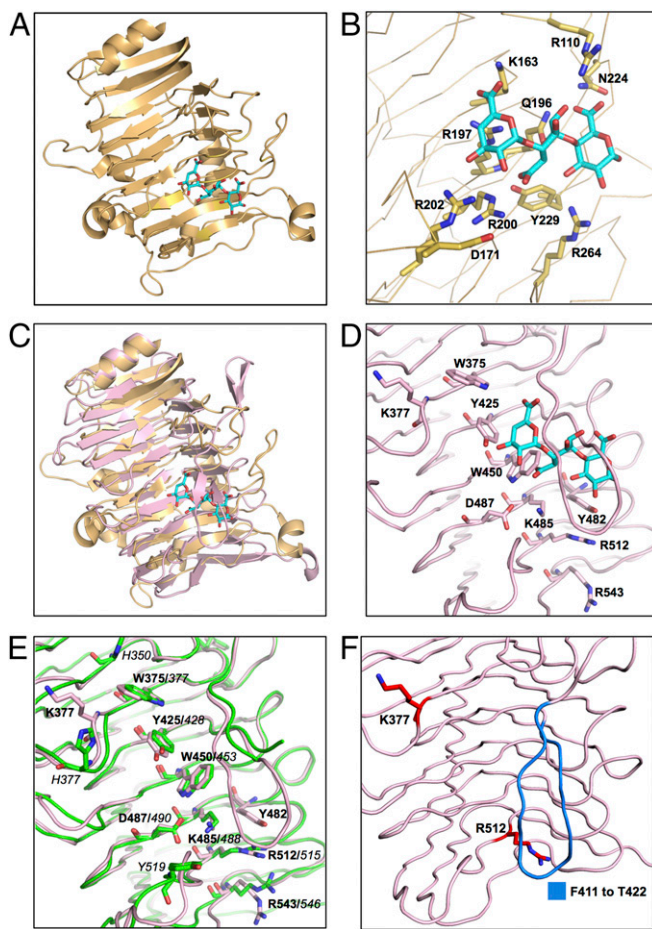


Fig. 3. Comparison of the TM-Pel-binding pocket with the PuBS of SRRP₅₃₆₀₈-BR and SRRP₁₀₀₋₂₃-BR. (A) Crystal structure of TM-Pel (Protein Data Bank ID code 3ZSC) (orange) in complex with TGA (cyan). (B) A close-up view of the TM-Pel-binding pocket, with residues involved in TGA binding represented as sticks. (C) Superposition of SRRP₅₃₆₀₈-BR₂₆₂₋₅₇₁ (light pink) and TM-Pel (orange) structures, with an rmsd of 2.63 over 210 residues, shows that the PuBS of the former overlaps with that of TM-Pel. (D) Surface-exposed aromatic and charged residues on PB3 in SRRP₅₃₆₀₈-BR₂₆₂₋₅₇₁ PuBS (light pink). This includes the aromatic residue triad W375, Y425, and W450 and the basic residue triad K485, R512, and R543. (E) Solvent-exposed residues of PuBS in the overlaid structures of SRRP₅₃₆₀₈-BR (light pink) and SRRP₁₀₀₋₂₃-BR (green), with an rmsd of 0.912 over 293 residues, showing that several solvent-exposed residues in both binding sites are conserved. Residues in bold are from SRRP₅₃₆₀₈-BR, and those in italic font are from SRRP₁₀₀₋₂₃-BR. (F) Residues mutated for functional analysis of SRRP₅₃₆₀₈-BR. Single mutants were created by substituting the residues in red (K377 or R512) with alanine. Residues in blue from F411 to T422 in the lower loop were deleted to generate the ΔF411-T422 deletion mutant.

Following the structural homology of SRRP₅₃₆₀₈-BR and SRRP₁₀₀₋₂₃-BR with PelC-like proteins, binding of SRRP₅₃₆₀₈-BR was performed with polygalacturonic acid (PGA)-containing pectin fragments using a carbohydrate array of well-characterized plant polysaccharides and oligosaccharides produced by partial hydrolysis from polysaccharides (43, 44). Interestingly the binding was found to be pH-dependent, with SRRP₅₃₆₀₈-BR showing specific and reproducible binding to pectin structures at pH 4.0 but not at pH 7.4 (*SI Appendix*, Fig. S8 and Table S4). In most cases, the glycans showing binding were lime pectin fractions with a low degree of esterification (DE ≤ 31%) of the galacturonic acid moieties present or PGA isolated from citrus pectin, whereas pectin fractions with higher DE values gave little or no binding. Such pH-dependent interaction was confirmed by bio-layer interferometry using the

Octet system where biotinylated-SRRP₅₃₆₀₈-BR was immobilized on streptavidin-coated optical biosensors and probed with rhamnogalacturonan I (RGI), pectin esterified from citrus fruit (PECF), or PGA as ligand. A sensorgram showing the rate of association (k_a) and rate of dissociation (k_d) of SRRP₅₃₆₀₈-BR binding to PGA or RGI at pH 4.0 is shown in *SI Appendix*, Fig. S9. The kinetic parameters for the interaction of SRRP₅₃₆₀₈-BR and PGA were determined through global fitting of raw data using a 1:1 (Langmuir) binding model with a $k_a = 3.03 \times 10^2 \text{ M}^{-1} \cdot \text{s}^{-1} \pm 0.54\%$ and $k_d = 7.17 \times 10^{-5} \text{ s}^{-1} \pm 0.69\%$, yielding an equilibrium dissociation constant, $K_d = 0.237 \times 10^{-6} \text{ M}$ with an R^2 of 0.997077 and full $\chi^2 = 0.23$ (Table 2), the latter two values confirming the fitting of the model (*SI Appendix*, Fig. S9A). While binding was observed with RGI at pH 4.0, it was not possible to fit an acceptable model to the data, although it is apparent that the interaction dissociates rapidly upon removal of the ligand (*SI Appendix*, Fig. S9B). Binding was not observed for two commercially available pectins, PECF and pectin P7536, both obtained from Sigma (*SI Appendix*, Fig. S9C). Additionally, no binding could be detected when the experiments were performed at pH 7.4. Preliminary screening assays using pH 7.4, 7.0, 6.5, 6.0, 5.5, 5.0, 4.5, and 4.0 demonstrated the pH-dependent increase in binding to PGA at lower pH (pH 5.0 and below). Initial assays omitting EDTA or Tween 20 in the run buffers resulted in nonspecific binding. As shown in Fig. 3, the superposition of the SRRP₅₃₆₀₈-BR₂₆₂₋₅₇₁ and TM-Pel-TGA

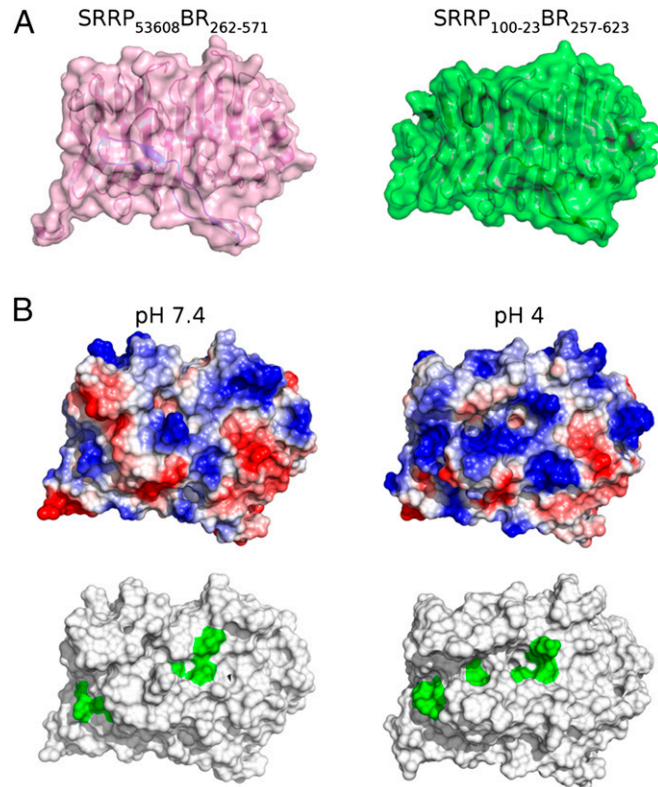


Fig. 4. The pH-dependent conformational change affects the PuBS, as predicted by MD simulations. (A) Combined surface and cartoon models of SRRP₅₃₆₀₈-BR₂₆₂₋₅₇₁ (pink) and SRRP₁₀₀₋₂₃-BR₂₅₇₋₆₂₃ (green). (B) Surface representation of SRRP₅₃₆₀₈-BR₂₆₂₋₅₇₁ at pH 7.4 and pH 4.0 in the same orientation as in A, showing surface electrostatics (Upper) and surface-exposed putative binding residues (Lower, green). At pH 4.0, PuBS exhibits a more positive electrostatic potential as well as an open conformation that exposes a greater number of putative binding residues to the solvent. Coordinates were obtained from representative frames of each respective MD trajectory (Methods). Surface electrostatics were calculated in PyMOL and are color-coded as blue (positive), white (neutral), and red (negative).

Table 2. Binding kinetics of SRRP₅₃₆₀₈-BR variants against PGA as analyzed by bio-layer interferometry

SRRP ₅₃₆₀₈ -BR variants	K_d (M)	k_a , M ⁻¹ ·s ⁻¹	k_a error	k_d , s ⁻¹	k_d error	Full χ^2	Full R ²
Wild-type	2.37E-07	3.03E+02	1.64E+00	7.17E-05	4.92E-06	0.231987	0.997077
Δ F411-T422	2.84E-06	3.14E+02	2.71E+00	8.91E-04	9.29E-06	0.314129	0.993248
R512A	4.66E-06	2.46E+02	2.59E+00	1.15E-03	1.03E-05	0.094123	0.992496
K377A	5.24E-06	2.58E+02	3.92E+00	1.35E-03	1.59E-05	0.114659	0.985439

structures allowed the identification of possible binding residues in SRRP₅₃₆₀₈-BR₂₆₂₋₅₇₁. To further investigate the specificity of the interaction, a series of SRRP₅₃₆₀₈-BR mutants was generated by site-directed mutagenesis (*Methods*, Fig. 3F, and *SI Appendix*) and tested against PGA. These included two alanine-substituted single mutants, K377A and R512A, and one where the lower loop from F411 to T422 was deleted, designated “ Δ F411-T422.” K377 and R512 were selected due to their localization at the extremities of the proposed PuBS. Furthermore, MD simulations also indicated a possible role of R512 in ligand binding. The Δ F411-T422 mutant was created to evaluate the importance of the flexible loop in ligand binding. All mutants showed similar circular dichroism spectra at pH 7.4, suggesting correct folding of the recombinant proteins (*SI Appendix*, Fig. S10). Additionally, no differences were observed between wild-type SRRP₅₃₆₀₈-BR at pH 7.4 and pH 4.0 (*SI Appendix*, Fig. S10). The mutations led to reduced K_d values, showing similar k_a but increased k_d , in comparison with the wild-type protein (Table 2). Chondroitin sulfate A (from bovine trachea) was also tested against immobilized SRRP₅₃₆₀₈-BR under the above conditions. Similarly, no binding was observed at pH 7.4. However, at pH 4.0, concentration-dependent binding could be observed with chondroitin sulfate A (*SI Appendix*, Fig. S9D). Binding analysis of chondroitin sulfate A (as above) determined a $k_a = 9.2 \times 10 \text{ M}^{-1} \cdot \text{s}^{-1} \pm 1.26\%$ and $k_d = 8.72 \times 10^{-5} \text{ s}^{-1} \pm 3.04\%$, yielding a $K_d = 9.47 \times 10^{-7} \text{ M}$ with an $R^2 = 0.9935$ and $\chi^2 = 0.21$.

L_rSRRP-BR Promotes *L. reuteri* Adhesion to the Intestinal Epithelium.

To determine the contribution of L_rSRRP-BR adherence to the host tissue following the reported ability of *L. reuteri* 100-23 (but not the *L. reuteri* 100-23 *rrp* mutant) to form biofilm in vivo (6), we performed adhesion assays to tissue sections of the mouse epithelium using soluble recombinant SRRP₅₃₆₀₈-BR at pH 7.4. Interestingly, we could detect binding of SRRP₅₃₆₀₈-BR to both stomach and colonic epithelium. In both types of tissue, the staining patterns correlated with wheat germ agglutinin (WGA) binding. No staining was observed in negative controls (SRRP₅₃₆₀₈-BR-free) (Fig. 5A and B). Binding of SRRP₅₃₆₀₈-BR to colonic tissue sections was significantly reduced following treatment with periodate at pH 4.0 (Fig. 5C), suggesting binding to glycoproteins. In the healthy stomach of mice and humans, the MUC5AC and MUC6 mucins dominate and are produced by the surface epithelium and glands, in line with the mucins produced by human HT-29-MTX cells. Direct binding of L_rSRRP-BR to the HT-29-MTX cells was carried out at pH 7.4. The SRRP₅₃₆₀₈-BR staining pattern correlated with WGA lectin and, to some degree, also with MUC5AC staining. No staining was observed in the negative control (SRRP₅₃₆₀₈-BR-free) (Fig. 5D). Furthermore, binding was also observed to HT-29 cell lines (Fig. 5E), suggesting that at pH 7.4 SRRP₅₃₆₀₈-BR can recognize mucins and/or other epithelial receptors.

To identify the nature of the ligands, we investigated the binding of SRRP₅₃₆₀₈-BR to individual components of the epithelium and mucus layer including purified mucins and DNA by atomic force microscopy (AFM). Compared with other techniques used to measure the force magnitude of ligand–receptor interactions, AFM provides specific information on the distance of interactions between molecules, i.e., the distance to the function-

alized tip as it moves along the immobilized ligand and retracts from the surface, as shown in the examples of force curves in Fig. 6, *Insets*. Fig. 6*A* shows quantification of the magnitude of adhesion captured in the retraction curves of the force spectroscopy measurements between SRRP₅₃₆₀₈-BR and mucin. In neutral buffer (pH 7.4) the modal value of adhesion events was 105 pN, whereas bimodal values of adhesion events, at 72 pN and 120 pN, were obtained in acidic buffer (pH 4.0). The addition of PGA appeared to abolish SRRP₅₃₆₀₈-BR–mucin interactions at pH 4.0, as PGA binds specifically to SRRP₅₃₆₀₈ only in acidic conditions. Furthermore, despite the adhesion magnitudes being similar in both buffers, the SRRP₅₃₆₀₈-BR and mucin interactions in the acidic buffer produced a significantly larger range of the length of adhesion events compared with the data obtained in neutral conditions (Fig. 6*B*). This suggests that SRRP₅₃₆₀₈-BR has a better ability to interact along the entire length of the mucin chains at acidic pH compared with neutral pH. Fig. 6*A* and *B* shows a set of the typical force–distance curves from each of the experiments to reveal the distance variations between pH 7.4 and 4.0. In Fig. 6*C*, direct binding of SRRP₅₃₆₀₈-BR to PGA was further confirmed by AFM at pH 4.0. There was a significantly large range of adhesion magnitudes, from 33–428 pN. The modal value was 36 pN at pH 4.0 and 18 pN in the neutral buffer, which corresponds to the noise level in the force spectra. Adding free PGA to the AFM liquid cell led to a significant reduction in adhesion events due to competitive interactions between free PGA and the glass-attached PGA molecules, as shown in the force curve example, thereby confirming the specificity of the interaction.

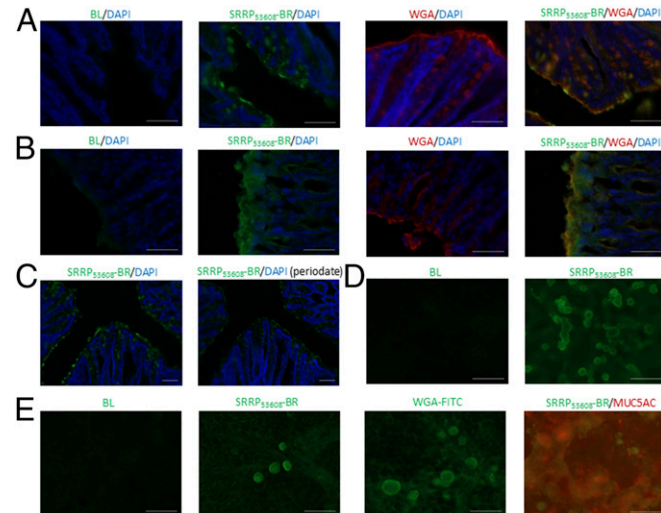


Fig. 5. Adhesion of SRRP₅₃₆₀₈-BR to GI tissue. (A and B) Immunostaining pattern for SRRP₅₃₆₀₈-BR on cryosections of mouse colon (A) and stomach (B) correlates with WGA lectin staining. (C) SRRP₅₃₆₀₈-BR binding to mouse colonic sections following sodium periodate treatment at pH 4.5 is significantly reduced. (D and E) SRRP₅₃₆₀₈-BR binds to epithelial cells HT29 (D) and mucus-producing HT29-MTX cells (E). The immunostaining pattern for SRRP₅₃₆₀₈-BR on HT29-MTX cells correlates with WGA lectin staining and partly with anti-MUC5AC staining. Cell nuclei of tissue sections were counterstained with DAPI. (Scale bars: 50 μm .)

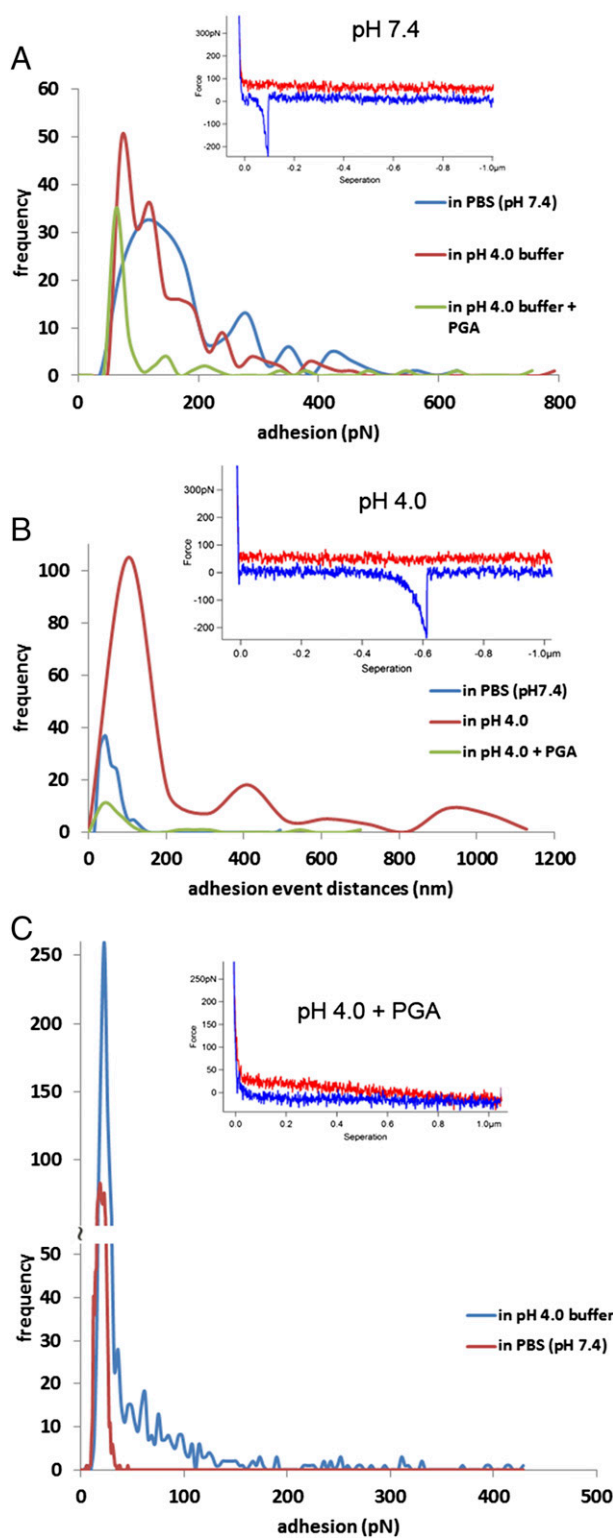


Fig. 6. AFM force spectroscopy histograms of SRRP₅₃₆₀₈-BR interacting with mucin or PGA. Insets show examples of force curves for each assay. (A) Quantification of adhesion values to mucin in buffers of neutral and acidic pH values or following PGA addition. (B) Quantification of variations in the mucin adhesion event distances. (C) Quantification of adhesion values to PGA in buffers of neutral and acidic pH values.

Force spectroscopy was also used to investigate the binding of SRRP₅₃₆₀₈-BR to DNA (Fig. 7). Increasing the NaCl molarity from 137 mM to 1 M in the PBS buffer caused a minor reduction

of the adhesion frequency (from 15 to 12) of SRRP₅₃₆₀₈-BR to DNA but increased the modal values of the adhesion events (from 123 to 160 pN) (Fig. 7*A*), suggesting that binding was unlikely to be solely due to electrostatic interactions. To further assess the specificity of the interaction between SRRP₅₃₆₀₈-BR and DNA, free DNA sample was added into the AFM liquid cell, resulting in a minor reduction of adhesion event frequency (from 33 to 30) and of modal values (from 83 to 60 pN) (Fig. 7*B*). Adding single nucleotides separately (Fig. 7 *C–E*) or in tandem (Fig. 7*F*, *Inset*) did not cause any major inhibition (only minor reductions in the frequency and modal values of the adhesions were observed). In contrast, the simultaneous addition of all four nucleotides led to a significant inhibition in terms of the adhesion event frequency (from 92 to 12) with similar modal values of adhesion (71 and 86 pN, respectively) (Fig. 7*F*), which is expected from single ligand–receptor interaction events as measured in the timescale of AFM experiments. These results suggest that all four nucleotides are recognized by SRRP₅₃₆₀₈-BR.

Discussion

Structural Differences Between SRRPs from Lactobacilli and Pathogenic Streptococci and Staphylococci Reflect Differences in Ligand Specificity. Bacterial attachment to host surfaces is a pivotal event in the biological and infectious processes of both commensal and pathogenic bacteria. SRRPs and their associated secretion systems are being defined in a growing number of Gram-positive bacteria, indicating their crucial roles in mediating interaction with the host.

Atomic-resolution structures of seven SRRP binding regions have been reported for Gram-positive pathogens to date, highlighting a relationship between their structural folds and binding ligands. These include *S. parasanguinis* Fap1 [Protein Data Bank (PDB) ID codes 2KUB and 2X12] (45), *S. gordonii* GspB (PDB ID code 3QC5/6) (13), *S. sanguinis* SrpA (PDB ID code 5EQ2) (46), Srr-1 and Srr-2 paralogues of *S. agalactiae* (PDB ID codes 4MBO/R) (47, 48), *S. aureus* SraP [PDB ID codes 4M0(0–3) (49), and *S. pneumoniae* PsrP (PDB ID codes 3ZGH/I) (50)]. Srr-1, Srr-2, and PsrP each adopt variations of the Dev-IgG fold (47, 50, 51) and bind to long β-strands in their target proteins, thereby forming a complementary strand along one of the Ig-like domains of the Dev-Ig protein, with Srr-1 binding to cytokeratin 4 (52–54), Srr-1 and Srr-2 binding to fibrinogen Aα (47, 55–58), and PsrP adhering to cytokeratin 10 (59) and to DNA (60). Other SRRP-BR regions are composed of two or more sub-domains and include (from the N to the C terminal) the helical and CnaA folds for Fap1 (45), the CnaA, sialic acid-binding Ig-like lectin (siglec), and unique subdomains for GspB (13), the siglec and unique subdomains for SrpA (46), and a legume lectin-like fold, a β-grasp fold, and two eukaryotic cadherin-like modules for SraP (49). The GspB, Hsa, SrpA, and SraP SRRP-BRs have all been shown to bind to different types of sialylated ligands (13, 49, 61–71), whereas the binding ligand of Fap1 remains to be identified (45). *LrSRRP*-BR did not recognize sialylated glycans but was found to bind to host epithelium or pectin-like components in a pH-dependent manner. This difference in ligand specificity can be explained by the *LrSRRP*-BR right-handed β-solenoid topology, which is typically adopted by extracellular, enzymatic PelC-like proteins. Such a fold has not previously been reported in SRRP-BRs and in proteins from *L. reuteri* species. Additionally, the *LrSRRP*-BR structural data indicate a high representation of Trp, Tyr, and basic residues in the PuBS, suggesting an involvement in carbohydrate binding, which may correlate with *LrSRRP*-BRs' recognition of mucin glycoproteins and plant-derived anionic polysaccharides. In addition, mutagenesis confirmed the importance of the binding loop and residues R512 and K377 within the PuBS in the interaction of SRRP₅₃₆₀₈-BR with PGA.

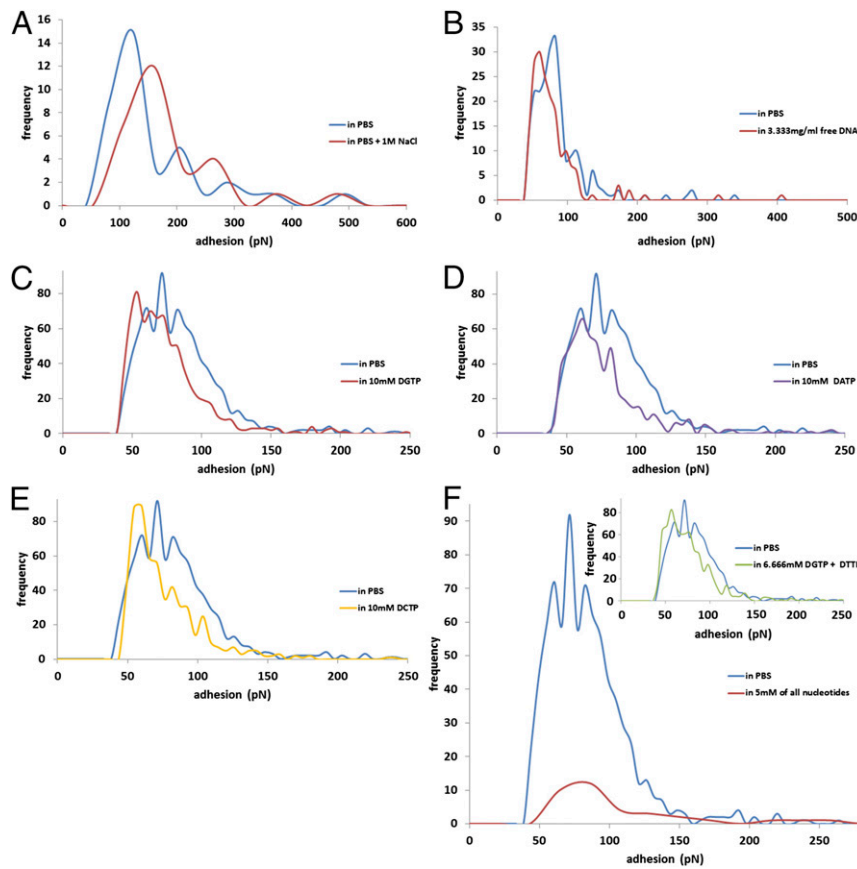


Fig. 7. AFM force spectroscopy histograms of SRRP₅₃₆₀₈-BR interacting with DNA. Quantification of adhesion values of SRRP₅₃₆₀₈-BR interacting with DNA in 137 mM NaCl or 1 M NaCl PBS (A) or after the addition of free DNA (B) or free nucleotides dGTP (C), dATP (D), dCTP (E), all four nucleotides (dGTP, dATP, dTTP, and dCTP) (F), or two nucleotides (dGTP and dTTP) (Inset in F).

LrSRRP-BR Binds to Polyanionic Ligands via a pH-Dependent Binding Mode.

Three major carbohydrate structures are found in pectin, which include homogalacturonan, RGI, and rhamnogalacturonan II. Strong pH dependency was observed when SRRP₅₃₆₀₈-BR binding was tested against chondroitin sulfate A and selected pectin ligands. SRRP₅₃₆₀₈-BR bound PGA and RGI at pH 4.0, but no binding was observed at pH 7.4 or against the two other commercial pectins tested at either pH. A similar preference for acidic pH was observed for binding to chondroitin sulfate A. Long MD simulations (at a microsecond timescale) at pH 4.0 and pH 7.4 showed that SRRP₅₃₆₀₈-BR undergoes a pH-dependent conformational change close to the PuBS, so that a greater region of the PuBS is solvent-exposed at pH 4.0. Coupled with a rearrangement of postulated key sidechains (D487, R512, I514, and Y482) at low pH, this suggests a mechanism for the observed differential binding to anionic PGA, RGI, and chondroitin sulfate A polysaccharides (*SI Appendix*, Fig. S11) at pH 4.0 and pH 7.4. Furthermore, the models suggest a notable difference in surface charge distribution in the PuBS at the two pH values, exhibiting a more positive potential at pH 4.0, which would certainly have a marked impact on the ability of SRRP₅₃₆₀₈-BR to bind anionic substrates. These results also suggest that other linear polyanionic glycosaminoglycan polysaccharides may be relevant biological ligands for SRRP in the gut. Such binding pH-dependent conformational change has previously been reported for the pectin lyase PelA (32) and also for the *S. parasanguinis* SRRP adhesin, Fap1, where the low-pH-driven conformational change modulates adhesion and likely plays a role in survival in acidic environments (72).

L. reuteri and many other *Lactobacillus* spp. are primary colonizers of the proximal GI tract and therefore are exposed to acidic stress in the stomach. The pH values in the rodent forestomach region range between 3.8 and 5.1 depending on feeding (73). Similarly, in the porcine stomach, the pH is relatively low at the esophageal terminus of the stomach and is higher toward the pylorus (74). In addition to a longitudinal pH gradient along the GI tract, there is a pH gradient across mucus, as demonstrated in rodents *in vivo*, supporting a role for this barrier in gastric mucosal protection (75, 76). Our findings that *Lr*SRRP-BR binds to dietary components at low pH and to the mucosal epithelium at higher pH are in line with the observed pH gradient from the lumen to the epithelium surface. It is also worth noting that in the stomach, the *Helicobacter pylori* sialic acid-binding adhesin (SabA) shows a charge/low-pH-dependent mechanism likely to play different roles during colonization of the oral to gastric niches and during long-term infection (77).

Lessons on Niche Specificity and Biofilm Formation. SRRPs comprise a large family of adhesins in Gram-positive bacteria (45) which are exported by an accessory Sec system (the SecA2-SecY2 system) (11) and are important for biofilm formation (64, 78, 79). Here we showed that in *L. reuteri* strains genes encoding homologs of SRRPs are generally colocalized within the SecA2-SecY2 gene cluster with only a few exceptions of unlinked SRRP genes or pseudogenes. While the overall domain organization of SRRPs is conserved between Gram-positive bacteria species, the individual SRRP-BR domains are highly diverse with limited to no sequence homology (80). SRRPs have been characterized from numerous streptococci and staphylococci inhabiting different

niches and contributing to pathogenesis due to their role in host cell adhesion and biofilm formation. Fap1 from *S. parasanguinis* (72, 81, 82) as well as the sialoglycan-binding SRR adhesins Hsa and GspB from *S. gordonii* strains CH1 and M99, respectively, are involved in dental plaque formation and periodontal disease via attachment to salivary components. They are also a virulence factor for infective endocarditis initiated by their binding to sialoglycans on human platelets. *S. sanguinis* and *S. aureus* are other pathogens causing bacterial endocarditis in which their SRR adhesins, SrpA and SraP, respectively, also mediate binding to sialylated receptors on human platelets (63, 83). Srr-1 and Srr-2 adhesins from the *S. agalactiae* pathogen, causing neonatal meningitis, bind to human fibrinogen and keratin 4. Keratin 4 binding mediates colonization of the female genital tract, leading to neonatal infection, and fibrinogen binding mediates adhesion to human brain microvascular endothelial cells (47, 55). PsrP from *S. pneumoniae*, causing streptococcal pneumonia, facilitates biofilm formation on lung epithelial cells via self-oligomerization, and by DNA binding and adhesion to keratin 10, both facilitated by its BR (50, 59, 62, 78). It is worth noting that SRRPs also occur in commensal streptococci based on sequence analysis and that SRR glycoproteins from *S. salivarius* were recently shown to play a major role in host colonization, although no structural information is available (14).

Here, we show that SRRP₅₃₆₀₈-BR from *L. reuteri* binds to the epithelium and dietary components in a pH-dependent mechanism, which may favor persistence in the GI tract. In addition to its role in adhesion to polysaccharides and glycoproteins, SRRP₅₃₆₀₈-BR could bind DNA in a specific manner, as shown by AFM. DNA from autolyzed bacterial cells is a component of many biofilms, helping form an extracellular network to which live cells can attach. This therefore may contribute to the ability of *L. reuteri* rodent strains (and perhaps other *Lactobacillus* spp. harboring SRRPs identified by bioinformatics analysis) to form biofilm on the murine forestomach *in vivo* (6). While pathogenic biofilms contribute to states of chronic inflammation, biofilm formation by probiotic bacteria such as *Lactobacillus* spp. causes a negligible immune response and is considered a beneficial property by promoting colonization and longer permanence in

the host mucosa and limiting colonization by pathogenic bacteria. Understanding at the molecular level the contribution of *Lactobacillus* SRRPs in biofilm formation is needed to fully exploit the functions of this intra- and interspecies family of adhesins across Gram-positive bacteria. These molecular findings may help the rational selection of probiotic strains of *Lactobacilli* that can compete with the SRRP-mediated adhesion of pathogenic streptococci and staphylococci.

Methods

Crystallization of SRRP₅₃₆₀₈-BR and SRRP₁₀₀₋₂₃-BR. Cloning, purification, crystallization, and structure determination are described in *SI Appendix*.

MD Simulations. Protein protonation states at pH 4.0 and 7.4 were predicted by Schrodinger's Maestro software suite (PROPKA module), and long MD simulations were run using AMBER 14. Details of the simulations are described in *SI Appendix*.

Binding Assays. Binding of SRRP₅₃₆₀₈-BR wild-type and mutants to PGA, RGI, pectins, and chondroitin sulfate A was performed by bio-layer interferometry. Binding of SRRP₅₃₆₀₈-BR to mucins, DNA, and PGA was assessed by force spectroscopy using AFM. Immunofluorescence was used to monitor SRRP₅₃₆₀₈-BR binding to mouse intestinal tissue sections as described in *SI Appendix*.

Full details of all experimental procedures used are described in *SI Appendix*.

ACKNOWLEDGMENTS. We thank Jens Walter for provision of *L. reuteri* strains; Zahra Khedri, Ajit Varki (University of California), and the Consortium for Functional Glycomics for testing the protein on their sialoglycan array and 5.1 mammalian glycan arrays, respectively; and the staff at I03 of Diamond Light Source UK for beamtime (Proposal mx9475) and their assistance with data collection. This work was supported by the Biotechnology and Biological Sciences Research Council (BBSRC) Institute Strategic Programme for the Gut Health and Food Safety Grant BB/J004529/1 and the BBSRC Responsive Mode Grant BB/K019554/1. S.S. was supported by a University of East Anglia Faculty of Medicine and Health Sciences studentship and in part by the Gen Foundation charitable trust. D.L. was supported by a PhD studentship with financial support from the Institute of Food Research/Quadrant Bioscience Institute Extra. J.A. and S.W. received funding from the BBSRC through Research Grant BB/P010660/1 and a Doctoral Training Partnership PhD studentship, respectively. C.D. is the recipient of Wellcome Trust Investigator Award WT106121MA.

1. Lynch SV, Pedersen O (2016) The human intestinal microbiome in health and disease. *N Engl J Med* 375:2369–2379.
2. Walter J, Britton RA, Roos S (2011) Host-microbial symbiosis in the vertebrate gastrointestinal tract and the *Lactobacillus reuteri* paradigm. *Proc Natl Acad Sci USA* 108: 4645–4652.
3. Walter J (2008) Ecological role of lactobacilli in the gastrointestinal tract: Implications for fundamental and biomedical research. *Appl Environ Microbiol* 74:4985–4996.
4. Oh PL, et al. (2010) Diversification of the gut symbiont *Lactobacillus reuteri* as a result of host-driven evolution. *ISME J* 4:377–387.
5. Frese SA, et al. (2011) The evolution of host specialization in the vertebrate gut symbiont *Lactobacillus reuteri*. *PLoS Genet* 7:e1001314.
6. Frese SA, et al. (2013) Molecular characterization of host-specific biofilm formation in a vertebrate gut symbiont. *PLoS Genet* 9:e1004057.
7. Duar RM, et al. (2017) Experimental evaluation of host adaptation of *Lactobacillus reuteri* to different vertebrate species. *Appl Environ Microbiol* 83:e00132-17.
8. Wegmann U, et al. (2015) The pan-genome of *Lactobacillus reuteri* strains originating from the pig gastrointestinal tract. *BMC Genomics* 16:1023.
9. Lizcano A, Sanchez CJ, Orihuela CJ (2012) A role for glycosylated serine-rich repeat proteins in gram-positive bacterial pathogenesis. *Mol Oral Microbiol* 27: 257–269.
10. Felthorpe ME, Braunstein M (2012) Emerging themes in SecA2-mediated protein export. *Nat Rev Microbiol* 10:779–789.
11. Prabudiansyah I, Driessens AJM (2017) The canonical and accessory Sec system of Gram-positive bacteria. *Curr Top Microbiol Immunol* 404:45–67.
12. Handley PS, Correia FF, Russell K, Rosan B, DiRienzo JM (2005) Association of a novel high molecular weight, serine-rich protein (SrpA) with fibril-mediated adhesion of the oral biofilm bacterium *Streptococcus crista*. *Oral Microbiol Immunol* 20: 131–140.
13. Pyburn TM, et al. (2011) A structural model for binding of the serine-rich repeat adhesin GspB to host carbohydrate receptors. *PLoS Pathog* 7:e1002112.
14. Couvigny B, et al. (2017) Three glycosylated serine-rich repeat proteins play a pivotal role in adhesion and colonization of the pioneer commensal bacterium, *Streptococcus salivarius*. *Environ Microbiol* 19:3579–3594.
15. Tytgat HL, de Vos WM (2016) Sugar coating the envelope: Glycoconjugates for microbe-host crosstalk. *Trends Microbiol* 24:853–861.
16. Roos S, Karner F, Axelsson L, Jonsson H (2000) *Lactobacillus mucosae* sp. nov., a new species with in vitro mucus-binding activity isolated from pig intestine. *Int J Syst Evol Microbiol* 50:251–258.
17. Su MS, Oh PL, Walter J, Gänzle MG (2012) Intestinal origin of sourdough *Lactobacillus reuteri* isolates as revealed by phylogenetic, genetic, and physiological analysis. *Appl Environ Microbiol* 78:6777–6780.
18. Lee JH, et al. (2012) Genome sequence of *Lactobacillus mucosae* LM1, isolated from piglet feces. *J Bacteriol* 194:4766.
19. Holm L, Rosenström P (2010) Dali server: Conservation mapping in 3D. *Nucleic Acids Res* 38:W545–W549.
20. Sillitoe I, et al. (2015) CATH: Comprehensive structural and functional annotations for genome sequences. *Nucleic Acids Res* 43:D376–D381.
21. Jenkins J, Pickersgill R (2001) The architecture of parallel beta-helices and related folds. *Prog Biophys Mol Biol* 77:111–175.
22. Kobe B, Kajava AV (2000) When protein folding is simplified to protein coiling: The continuum of solenoid protein structures. *Trends Biochem Sci* 25:509–515.
23. Yoder MD, Keen NT, Jurnak F (1993) New domain motif: The structure of pectate lyase C, a secreted plant virulence factor. *Science* 260:1503–1507.
24. Akita M, Suzuki A, Kobayashi T, Ito S, Yamane T (2001) The first structure of pectate lyase belonging to polysaccharide lyase family 3. *Acta Crystallogr D Biol Crystallogr* 57:1786–1792.
25. Pickersgill R, Jenkins J, Harris G, Nasser W, Robert-Baudouy J (1994) The structure of *Bacillus subtilis* pectate lyase in complex with calcium. *Nat Struct Biol* 1:717–723.
26. Seyedarabi A, et al. (2010) Structural insights into substrate specificity and the anti beta-elimination mechanism of pectate lyase. *Biochemistry* 49:539–546.
27. Zheng Y, et al. (2012) Crystal structure and substrate-binding mode of a novel pectate lyase from alkaliphilic *Bacillus* sp. N16-5. *Biochem Biophys Res Commun* 420:269–274.
28. Creze C, et al. (2008) The crystal structure of pectate lyase PelI from soft rot pathogen *Erwinia chrysanthemi* in complex with its substrate. *J Biol Chem* 283:18260–18268.
29. Jenkins J, Shevchik VE, Hugouvieux-Cotte-Pattat N, Pickersgill RW (2004) The crystal structure of pectate lyase Pel9A from *Erwinia chrysanthemi*. *J Biol Chem* 279: 9139–9145.

30. Scavetta RD, et al. (1999) Structure of a plant cell wall fragment complexed to pectate lyase C. *Plant Cell* 11:1081–1092.
31. McDonough MA, et al. (2002) Crystallization and preliminary X-ray characterization of a thermostable pectate lyase from *Thermotoga maritima*. *Acta Crystallogr D Biol Crystallogr* 58:709–711.
32. Mayans O, et al. (1997) Two crystal structures of pectin lyase A from *Aspergillus* reveal a pH driven conformational change and striking divergence in the substrate-binding clefts of pectin and pectate lyases. *Structure* 5:677–689.
33. Vitali J, Schick B, Kester HC, Visser J, Jurnak F (1998) The tree-dimensional structure of *Aspergillus niger* pectin lyase B at 1.7-A resolution. *Plant Physiol* 116:69–80.
34. Petersen TN, Kauppinen S, Larsen S (1997) The crystal structure of rhamnogalacturonase A from *Aspergillus aculeatus*: A right-handed parallel beta helix. *Structure* 5: 533–544.
35. Mohnen D (2008) Pectin structure and biosynthesis. *Curr Opin Plant Biol* 11:266–277.
36. Yoder MD, Lietzke SE, Jurnak F (1993) Unusual structural features in the parallel beta-helix in pectate lyases. *Structure* 1:241–251.
37. Emsley P, Charles IG, Fairweather NF, Isaacs NW (1996) Structure of *Bordetella pertussis* virulence factor P69 pertactin. *Nature* 381:90–92.
38. Steinbacher S, et al. (1996) Crystal structure of phage P22 tailspike protein complexed with *Salmonella* sp. O-antigen receptors. *Proc Natl Acad Sci USA* 93:10584–10588.
39. Clantin B, et al. (2004) The crystal structure of filamentous hemagglutinin secretion domain and its implications for the two-partner secretion pathway. *Proc Natl Acad Sci USA* 101:6194–6199.
40. Locht C, Bertin P, Menozzi FD, Renaud G (1993) The filamentous haemagglutinin, a multifaceted adhesion produced by virulent *Bordetella* spp. *Mol Microbiol* 9:653–660.
41. Deng L, Chen X, Varki A (2013) Exploration of sialic acid diversity and biology using sialoglycan microarrays. *Biopolymers* 99:650–665.
42. Padler-Karavani V, et al. (2012) Cross-comparison of protein recognition of sialic acid diversity on two novel sialoglycan microarrays. *J Biol Chem* 287:22593–22608.
43. Pedersen HL, et al. (2012) Versatile high resolution oligosaccharide microarrays for plant glyobiology and cell wall research. *J Biol Chem* 287:39429–39438.
44. Sørensen I, Pedersen HL, Willats WG (2009) An array of possibilities for pectin. *Carbohydr Res* 344:1872–1878.
45. Ramboarina S, et al. (2010) Structural insights into serine-rich fimbriae from Gram-positive bacteria. *J Biol Chem* 285:32446–32457.
46. Bensing BA, et al. (2016) Structural basis for sialoglycan binding by the *Streptococcus sanguinis* SrpA adhesin. *J Biol Chem* 291:7230–7240.
47. Seo HS, et al. (2013) Characterization of fibrinogen binding by glycoproteins Srr1 and Srr2 of *Streptococcus agalactiae*. *J Biol Chem* 288:35982–35996.
48. Sundaresan R, Samen U, Ponnuraj K (2011) Expression, purification, crystallization and preliminary X-ray diffraction studies of the human keratin 4-binding domain of serine-rich repeat protein 1 from *Streptococcus agalactiae*. *Acta Crystallogr Sect F Struct Biol Cryst Commun* 67:1582–1585.
49. Yang YH, et al. (2014) Structural insights into SrpA-mediated *Staphylococcus aureus* adhesion to host cells. *PLoS Pathog* 10:e1004169.
50. Schulte T, et al. (2014) The basic keratin 10-binding domain of the virulence-associated pneumococcal serine-rich protein PsrP adopts a novel MSCRAMM fold. *Open Biol* 4:130090.
51. Sundaresan R, Samen U, Ponnuraj K (2015) Structure of KRT4 binding domain of Srr-1 from *Streptococcus agalactiae* reveals a novel β-sheet complementation. *Int J Biol Macromol* 75:97–105.
52. Samen U, Eikmanns BJ, Reinscheid DJ, Borges F (2007) The surface protein Srr-1 of *Streptococcus agalactiae* binds human keratin 4 and promotes adherence to epithelial HEp-2 cells. *Infect Immun* 75:5405–5414.
53. Sheen TR, et al. (2011) Serine-rich repeat proteins and pili promote *Streptococcus agalactiae* colonization of the vaginal tract. *J Bacteriol* 193:6834–6842.
54. Wang NY, et al. (2014) Group B streptococcal serine-rich repeat proteins promote interaction with fibrinogen and vaginal colonization. *J Infect Dis* 210:982–991.
55. Seo HS, Mu R, Kim BJ, Doran KS, Sullam PM (2012) Binding of glycoprotein srr1 of *Streptococcus agalactiae* to fibrinogen promotes attachment to brain endothelium and the development of meningitis. *PLoS Pathog* 8:e1002947.
56. Seo HS, Xiong YQ, Sullam PM (2013) Role of the serine-rich surface glycoprotein Srr1 of *Streptococcus agalactiae* in the pathogenesis of infective endocarditis. *PLoS One* 8:e64204.
57. Six A, et al. (2015) Srr2, a multifaceted adhesin expressed by ST-17 hypervirulent group B Streptococcus involved in binding to both fibrinogen and plasminogen. *Mol Microbiol* 97:1209–1222.
58. van Sorge NM, et al. (2009) The group B streptococcal serine-rich repeat 1 glycoprotein mediates penetration of the blood-brain barrier. *J Infect Dis* 199:1479–1487.
59. Shivshankar P, Sanchez C, Rose LF, Orihuela CJ (2009) The *Streptococcus pneumoniae* adhesin PsrP binds to Keratin 10 on lung cells. *Mol Microbiol* 73:663–679.
60. Schulte T, et al. (2016) The BR domain of PsrP interacts with extracellular DNA to promote bacterial aggregation; structural insights into pneumococcal biofilm formation. *Sci Rep* 6:32371.
61. Bensing BA, et al. (2016) Novel aspects of sialoglycan recognition by the Siglec-like domains of streptococcal SRR glycoproteins. *Glycobiology* 26:1222–1234.
62. Muller YA (2013) Unexpected features in the Protein Data Bank entries 3qd1 and 4i8e: The structural description of the binding of the serine-rich repeat adhesin GspB to host cell carbohydrate receptor is not a solved issue. *Acta Crystallogr Sect F Struct Biol Cryst Commun* 69:1071–1076.
63. Deng L, et al. (2014) Oral streptococci utilize a Siglec-like domain of serine-rich repeat adhesins to preferentially target platelet sialoglycans in human blood. *PLoS Pathog* 10:e1004540.
64. Kim AR, et al. (2016) Serine-rich repeat adhesin gordonii surface protein B is important for *Streptococcus gordonii* biofilm formation. *J Endod* 42:1767–1772.
65. Oguchi R, et al. (2016) Contribution of *Streptococcus gordonii* Hsa adhesin to biofilm formation. *Jpn J Infect Dis* 70:399–404.
66. Takahashi Y, et al. (2006) Contribution of sialic acid-binding adhesin to pathogenesis of experimental endocarditis caused by *Streptococcus gordonii* DL1. *Infect Immun* 74: 740–743.
67. Takamatsu D, et al. (2005) Binding of the *Streptococcus gordonii* surface glycoproteins GspB and Hsa to specific carbohydrate structures on platelet membrane glycoprotein Ibalpha. *Mol Microbiol* 58:380–392.
68. Takamatsu D, Bensing BA, Prakophol A, Fisher SJ, Sullam PM (2006) Binding of the streptococcal surface glycoproteins GspB and Hsa to human salivary proteins. *Infect Immun* 74:1933–1940.
69. Urano-Tashiro Y, Takahashi Y, Oguchi R, Konishi K (2016) Two arginine residues of *Streptococcus gordonii* sialic acid-binding adhesin Hsa are essential for interaction to host cell receptors. *PLoS One* 11:e0154098.
70. Yajima A, et al. (2008) Hsa, an adhesin of *Streptococcus gordonii* DL1, binds to alpha2-3-linked sialic acid on glycophorin A of the erythrocyte membrane. *Microbiol Immunol* 52:69–77.
71. Loukachevitch LV, et al. (2016) Structures of the *Streptococcus sanguinis* SrpA binding region with human sialoglycans suggest features of the physiological ligand. *Biochemistry* 55:5927–5937.
72. Garnett JA, et al. (2012) Structural insight into the role of *Streptococcus parasanguinis* Fap1 within oral biofilm formation. *Biochem Biophys Res Commun* 417:421–426.
73. Ward FW, Coates ME (1987) Gastrointestinal pH measurement in rats: Influence of the microbial flora, diet and fasting. *Lab Anim* 21:216–222.
74. Jubb K, Kennedy P, Palmer N (1992) *Pathology of Domestic Animals* (Academic, San Diego), 4th Ed, Vol 2.
75. McNeil NI, Ling KLE, Wager J (1987) Mucosal surface pH of the large intestine of the rat and of normal and inflamed large intestine in man. *Gut* 28:707–713.
76. Schreiber S, et al. (2004) The spatial orientation of *Helicobacter pylori* in the gastric mucus. *Proc Natl Acad Sci USA* 101:5024–5029.
77. Lindén SK, Wickström C, Lindell G, Gilshenan K, Carlstedt I (2008) Four modes of adhesion are used during *Helicobacter pylori* binding to human mucins in the oral and gastric niches. *Helicobacter* 13:81–93.
78. Sanchez CJ, et al. (2010) The pneumococcal serine-rich repeat protein is an intra-species bacterial adhesin that promotes bacterial aggregation in vivo and in biofilms. *PLoS Pathog* 6:e1001044.
79. Bandara M, et al. (2017) The accessory Sec system (SecY2A2) in *Streptococcus pneumoniae* is involved in export of pneumolysin toxin, adhesion and biofilm formation. *Microbes Infect* 19:402–412.
80. Zhou M, Wu H (2009) Glycosylation and biogenesis of a family of serine-rich bacterial adhesins. *Microbiology* 155:317–327.
81. Chen Q, Sun B, Wu H, Peng Z, Fives-Taylor PM (2007) Differential roles of individual domains in selection of secretion route of a *Streptococcus parasanguinis* serine-rich adhesin, Fap1. *J Bacteriol* 189:7610–7617.
82. Wu H, Zeng M, Fives-Taylor P (2007) The glycan moieties and the N-terminal polypeptide backbone of a fimbria-associated adhesin, Fap1, play distinct roles in the biofilm development of *Streptococcus parasanguinis*. *Infect Immun* 75:2181–2188.
83. Siboo IR, Chambers HF, Sullam PM (2005) Role of SrpA, a serine-rich surface protein of *Staphylococcus aureus*, in binding to human platelets. *Infect Immun* 73:2273–2280.